Journal of Power Sources 199 (2012) 201–206

Contents lists available at SciVerse ScienceDirect

Journal of Power Sources

journal homepage: www.elsevier.com/locate/jpowsour

Structural analysis, phase stability and electrochemical characterization of Nb doped $BaCe_{0.9}Y_{0.1}O_{3-x}$ electrolyte for IT-SOFCs

Elisabetta Di Bartolomeo[a,*], Alessandra D'Epifanio[a], Chiara Pugnalini[a], Francesco Giannici[b], Alessandro Longo[c], Antonino Martorana[b], Silvia Licoccia[a]

[a] Dipartimento di Scienze e Tecnologie Chimiche e Centro NAST, Università di Roma Tor Vergata, Via della Ricerca Scientifica 1, 00133 Roma, Italy
[b] Dipartimento di Chimica "Stanislao Cannizzaro", Università di Palermo, Viale delle Scienze, I-90128 Palermo, Italy
[c] Istituto per lo Studio dei Materiali Nanostrutturati, Consiglio Nazionale delle Ricerche, Via Ugo La Malfa, 153, I-90146 Palermo, Italy

ARTICLE INFO

Article history:
Received 20 July 2011
Received in revised form
30 September 2011
Accepted 11 October 2011
Available online 17 October 2011

Keywords:
High temperature proton conductors (HTPCs)
Barium cerates
Nb-doping
Structural analysis
Electrochemical performance

ABSTRACT

To improve the chemical stability of high temperature proton conductors based on barium cerate, electrolyte powders doped with different amounts of niobium were synthesized by the citrate–nitrate auto-combustion method. Pure single phases of $BaCe_{0.9-x}Nb_xY_{0.1}O_{3-x}$ (BCYN, $0.03 \le x \le 0.12$) were obtained by thermal treatment at 1000 °C. Sintering at 1450 °C for 10 h produced dense pellets. X-ray absorption spectroscopy allowed to define the dopant ion insertion site and the co-dopant valency. Treatments in pure CO_2 atmosphere at 700 °C for 3 h and subsequent XRD analysis were carried out to probe the chemical stability of the produced electrolytes. The influence of the presence of Nb^{5+} on conductivity has been investigated by electrochemical impedance spectroscopy (EIS) measurements. Polarization curves were acquired in the 400–750 °C temperature range.

1. Introduction

Essential requirements that must be met by high temperature proton conducting (HTPC) perovskite oxides for the application as electrolytes in solid oxide fuel cells operating at intermediate temperature ($450 \le T \le 750$ °C, IT-SOFC) are high proton conductivity coupled with structural and chemical stability in different atmospheres under fuel cell operating conditions [1,2]. Electrolyte materials must be characterized by thermodynamic or at least long-term kinetic stability in both anodic and cathodic SOFC environments. The requirement for high proton conductivity is met by barium cerate based materials [3–5], but their good proton transport features are coupled with chemical instability in the presence of acidic gases (e.g., CO_2 and SO_2) and water [6,7], hence they are not suitable for practical applications. Among the different strategies that have been followed to improve the stability of barium cerate-based, a widespread one has been doping the materials with different cations [8–12]. Different authors have investigated solid solutions of doped barium cerate and barium zirconate [13–18]. Given that the Zr^{4+} ionic radius is smaller than that of Ce^{4+}, a decrease of the unit cell volume of $BaCeO_3$ has been observed with increasing Zr content, corresponding to improved stability in the presence of carbon dioxide and water vapour, but also to concomitant decrease in conductivity.

Protecting a pellet of 20 mol% Y-doped barium cerate (BCY20) electrolyte with a thin layer of 20 mol% Y-doped barium zirconate (BZY20) has been reported to be effective in preventing the reaction of BCY20 with CO_2 without significantly reducing its electrical conductivity [19].

This paper reports on the attempt of improving the chemical stability of BCY by co-doping the perovskite structure's B site of with Nb^{5+}. The ionic radius (0.64 nm) of Nb^{5+} is smaller than both those of Ce^{4+} (B-site, 0.87 nm) and Y^{3+} (dopant cation, 0.90 nm) so that its introduction in the structure was expected to reduce the unit cell, hence to stabilize the compound against carbonation. Furthermore, being the niobium more electronegative than cerium, the acid characteristic of the doped species was expected to be more pronounced than those of the parent oxide [12,20]. At the same time, however, it must be considered that the insertion of the smaller Nb^{5+} in the B site neutralizes the anion vacancy brought about by an Y^{3+}, thus having a negative influence on the proton conductivity [12]. To investigate the balance between these two effects, $BaCe_{0.9-x}Nb_xY_{0.1}O_{3-x}$ (BCNY) powders with $0.03 \le x \le 0.12$ were synthesized by and sintered at the lowest

* Corresponding author. Tel.: +39 06 7259 4495; fax: +39 06 7259 4495.
E-mail address: dibartolomeo@uniroma2.it (E. Di Bartolomeo).

0378-7753/$ – see front matter © 2011 Elsevier B.V. All rights reserved.
doi:10.1016/j.jpowsour.2011.10.038

temperature necessary to obtain a dense microstructure. Their chemical stability was investigated by exposing the materials to pure CO_2 atmosphere at 700 °C, i.e. in conditions harsher than those occurring in a real FC device. The electrochemical characteristics of doped perovskites were investigated by electrochemical impedance spectroscopy (EIS) measurements and hydrogen–air fuel cell tests in the temperature range 400–750 °C.

2. Experimental

Oxide powders were prepared by citrate–nitrate auto-combustion method using $Ba(NO_3)_2$ (Aldrich, 99.999%), $Ce(NO_3)_2{\cdot}6H_2O$ (Aldrich, 99.999%), $Y(NO_3)_2{\cdot}6H_2O$ (Aldrich, 99.9%) and $C_4H_4NNbO_9{\cdot}xH_2O$ as starting reactants and citric acid as chelating agent and organic fuel. The synthetic procedure has been described in detail elsewhere [21]. $BaCe_{0.9-x}Nb_xY_{0.1}O_{3-x}$ (BCNY) powders with compositions ranging between 0.03 and 0.12 were prepared and labeled as in the following: BCYN1 ($x = 0.03$), BCYN2 ($x = 0.06$), BCYN3 ($x = 0.09$) and BCYN4 ($x = 0.12$). The powders were fired at 1000 °C for 10 h and characterized by X-ray diffraction (XRD, Philips X-Pert Pro 500 diffractomer with Cu Kα radiation) analysis. The chemical composition of the prepared compounds was analyzed by inductively coupled plasma optical emission spectrometry (ICP-OES, Varian Vista-MPX, CCD Simultaneous ICP-OES.).

X-ray absorption measurements on the Nb K-edge (19 keV) were carried out at the BM1 beamline of the European synchrotron radiation facility (ESRF, Grenoble, France) and at the XAFS beamline of Elettra (Trieste, Italy). Measurements were taken in transmission mode at 80 K using a liquid nitrogen cryostat on self-sustaining pellets mixed with cellulose. A niobium foil was mounted as a reference for the energy scale downstream from the sample. NbO_2 and Nb_2O_5 were used as standards for the X-ray absorption near-edge structure (XANES). The extended X-ray absorption fine structure (EXAFS) data were extracted and fitted with Viper [22], using theoretical phases and amplitudes calculated with FEFF8.4 [23]. The data were fitted in Fourier-transformed R-space from 0.8 to 4.5 Å, including the first three main peaks in the R-space plot.

Dense samples were obtained by uniaxially pressing (220 MPa) the powders into pellets (13 mm of diameter) and sintering at 1450 °C for 10 h. Pellets density was measured by picnometer (Mettler Toledo EL204). All samples showed relative densities above 90%. Pellets morphology was analyzed by field emission scanning electron microscopy (FE-SEM, Leo Supra 1250).

Electrochemical impedance spectroscopy (EIS) measurements were carried out in the 400–700 °C temperature range using a frequency response analyzer (FRA Solartron 1260), coupled with a dielectric interface (Solartron 1296), in a frequency range between 0.1 Hz and 10 MHz with an AC voltage amplitude of 100 mV. Gold wires were fixed with a drop of platinum paste (Engelhard-Clal) on the top of Pt electrodes and used as current collectors. The measurements were performed in different atmospheres. The gases were synthetic air (21% O_2/N_2), pure Ar, 5 vol.% of H_2 in Ar (all from Rivoira). The gases were either passed to the reactor directly (named "dry") or first humidified ("wet") to 3 vol.% of water content by passage through a water saturator held at room temperature. Flow rates were 100 ml min^{-1} for all gases.

Hydrogen–air fuel cell experiments were carried out in the temperature range 550–750 °C. Single cells were prepared with 0.6 mm thick electrolytes. Both anode and cathode were made of Pt using the above described preparation. During fuel cell operation, the anode surface was exposed to wet hydrogen (3 vol.% H_2O) and the cathode to ambient air. Measurements were performed with a Multichannel Potentiostat VMP3 (Princeton Applied Research).

Table 1
Composition of $BaCe_{0.9-x}Nb_xY_{0.1}O_{3-x}$ (prepared by Pechini method) after calcination at 1000 °C for 10 h.

Sample label	Composition
BCYN1	$BaCe_{0.87}Nb_{0.03}Y_{0.1}$
BCYN2	$BaCe_{0.84}Nb_{0.06}Y_{0.1}$
BCYN3	$BaCe_{0.81}Nb_{0.09}Y_{0.1}$
BCYN4	$BaCe_{0.78}Nb_{0.12}Y_{0.1}$

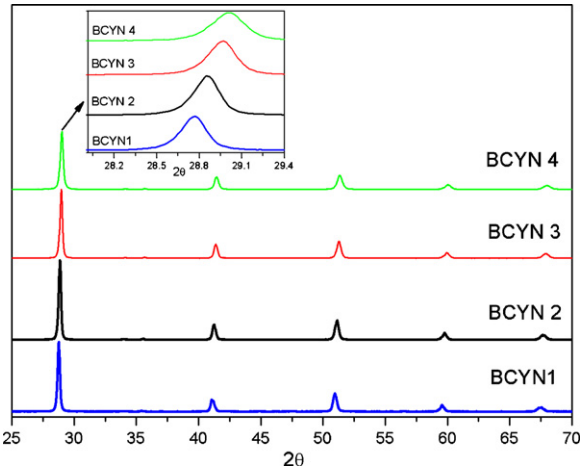

Fig. 1. XRD patterns of: BCYN compounds with different Nb molar contents calcined at 1000 °C and enlargement around $2\theta = 41°$.

3. Results and discussion

The composition of the $BaCe_{0.9-x}Nb_xY_{0.1}O_{3-x}$ oxides calcined at 1000 °C for 10 h was confirmed by ICP analysis and they are reported in Table 1. Fig. 1 shows the XRD patterns of BCYN compounds after calcination. A single orthorhombic phase (JCPDS 81-1386) was obtained for all different compositions. Increasing the Nb content, a slight shift at higher 2θ values was observed in the XRD patterns reported in the inset of Fig. 1, indicating that doping resulted in a change of the lattice parameters due to the insertion of niobium in the host barium cerate matrix.

The near-edge features of the X-ray absorption spectrum (XANES) provide valuable information on the electronic state of niobium in BCYN. In particular, it can be appreciated from the plot that the absorption edge energy increases with the oxidation state, as it is expected (in particular, the NbO_2 absorption edge is a few

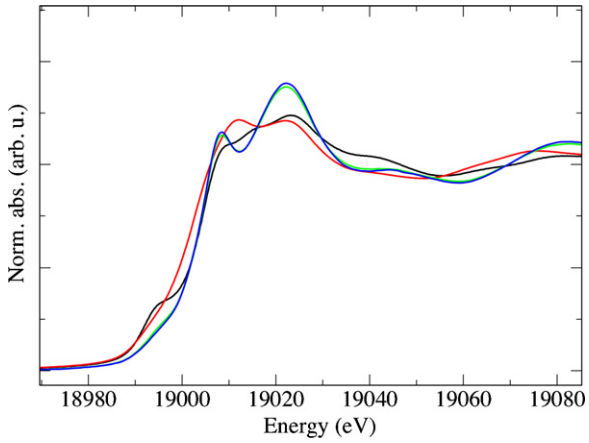

Fig. 2. K-edge XANES spectra of BCYN2 (blue) and BCYN4 (green). Reference K-edges of NbO_2 (red) and Nb_2O_5 (black) are also shown. (For interpretation of the references to color in this figure legend, the reader is referred to the web version of the article.)

Table 2
Results of the EXAFS data analysis. Coordination distances R are reported in Å and Debye–Waller factors σ^2 in 10^{-3} Å^2. Uncertainties are on the last digit.

	BCYN2 (80 K)	BCYN3 (80 K)	BCYN4 (80 K)
6 × Nb–O			
R	2.01	2.01	2.02
σ^2	7.2	7.3	9.0
8 × Nb–Ba			
R	3.67	3.69	3.70
σ^2	9.8	9.9	11
6 × Nb–M			
R	4.21	4.20	4.22
σ^2	5.1	5.1	4.6
12 × Nb–O			
R	4.64	4.61	4.52
σ^2	7.2	7.3	9.0

eV lower than Nb_2O_5). Nb^{3+} would show an absorption edge at even lower energies. It can be concluded that niobium in BCYN is in the Nb^{5+} state. Moreover, an inspection of the pre-edge region reveals that Nb_2O_5 has a prominent peak at about 18,995 eV, which is absent in the BCYN samples. Thus, it can also be concluded that niobium is dispersed in the barium cerate matrix, rather than being segregated in niobium oxide nano-domains (Fig. 2).

The EXAFS analysis was carried out as follows. A cubic perovskite model was used to build the scattering paths around niobium [24]. In this model, the Nb atom is placed in a regular perovskite B-site, so that the scattering paths around the absorbing atom are: (a) Nb-O_1 first shell, with Nb–O_1–Nb–O_1 intraoctahedral colinear multiple scattering; (b) Nb–Ba second shell, with cubic shape; (c) Nb–M (M = Ce, Y, Nb) third shell, including also Nb–O_1–M colinear multiple scattering configurations; (d) Nb–O_2 fourth shell, whose O_2 atom belongs to a neighboring octahedron. This cubic model involves the least number of parameters, compared with other perovskite models (i.e. orthorhombic), but it is nevertheless capable of satisfactorily fitting the experimental data. Assuming that intrinsic defectivity is much lower than the accuracy on refined coordination numbers, these were not refined during the fitting, as it is a standard practice with bulk compounds. An example of fitting is given in Fig. 3 and the overall results are reported in Table 2.

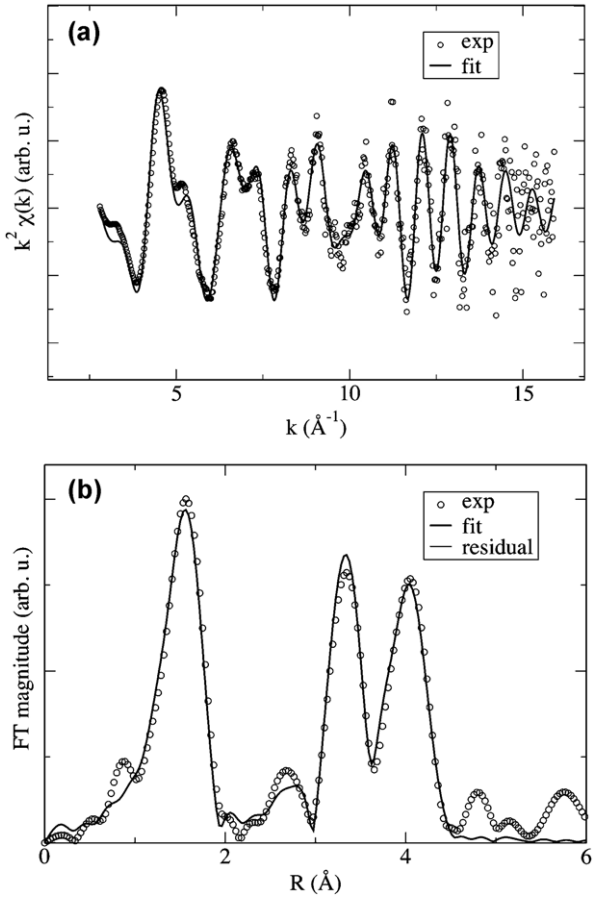

Fig. 3. EXAFS analysis of BCYN2. (a) k^2-Weighted EXAFS experimental (dots) and calculated (solid line) signal, (b) corresponding Fourier Transform magnitudes.

The Ce correlation distances in $BaCeO_3$, are about 2.25 Å (Ce–O), 3.71 Å and 3.85 Å (the two distances of Ce–Ba) and 4.43 Å (Ce–M, M = Ce, Y) [25]. By comparison with the results reported above, it is evident that the local structure of cerate is contracted around

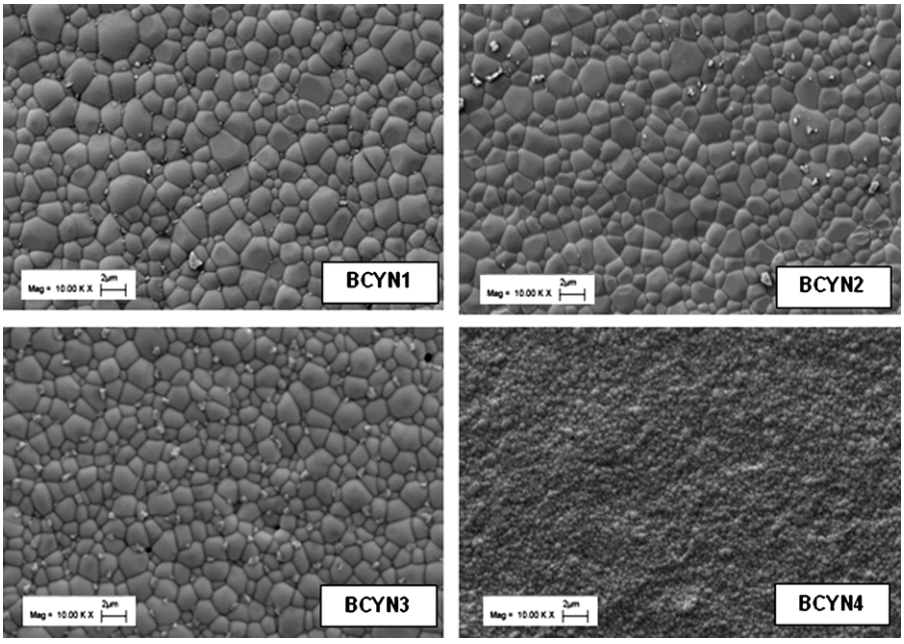

Fig. 4. FE-SEM of BCYN compounds with different Nb molar contents sintered at 1450 °C for 10 h.

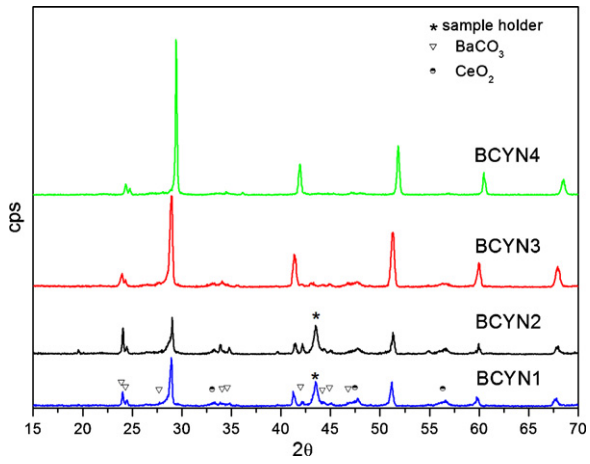

Fig. 5. XRD patterns of BCYN compounds with different Nb molar contents after CO_2 exposition.

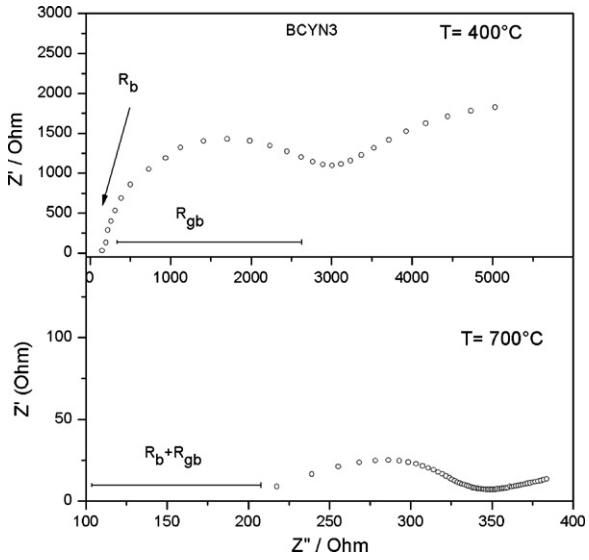

Fig. 6. Impedance spectra of BNYN3 sample measured at low (400 °C) and high (700 °C) temperatures in dry argon.

niobium. Moreover, the local symmetry is remarkably increased from orthorhombic to cubic, an evidence already observed in the case of In^{3+} doping in barium cerate [26]. As it is always the case with doped perovskites, the amount of dopant (in this case, niobium) generally increases the lattice disorder, as it is evident from the data reported in Table 2.

In conclusion, by X-ray absorption it is demonstrated that pentavalent niobium is inserted in the barium cerate B site producing a local contraction around niobium and a structural disorder increasing with the dopant concentration. XRD data analysis evidences the corresponding long-range structure shrinking and the presence of a single BCYN phase for all the investigated compositions.

Fig. 4 shows the FE-SEM micrographs of the powders after sintering. All pellets showed dense microstructures, confirming the relative density measurements. At variance with BCYN1, BCYN2 and BCYN3, which showed grain size in the range 1–2 μm, the morphology of BCYN4 appears to be drastically decreased to a submicrometric size.

The chemical stability of the compounds was investigated by exposing the sintered pellets to pure CO_2 atmosphere at 700 °C for 3 h, i.e. in a much harsher environment with respect to fuel cell operating conditions. Fig. 5 shows the XRD patterns of BCYN compounds after CO_2 treatment showing an increased chemical stability for higher Nb-content, confirming the positive effect of the oxide reduced basicity.

Impedance spectra collected for all samples were modeled as an equivalent circuit and conductivity values were extracted for the overall electrolyte. Fig. 6 shows typical impedance spectra of samples measured at low (400 °C) and high (700 °C) temperatures. At low temperatures $T < 450$–500 °C, depending on the pellets composition and the atmosphere, the Nyquist plots showed separated bulk and grain boundary contributions while at higher temperatures ($T > 500$ °C) only the total resistance could be measured.

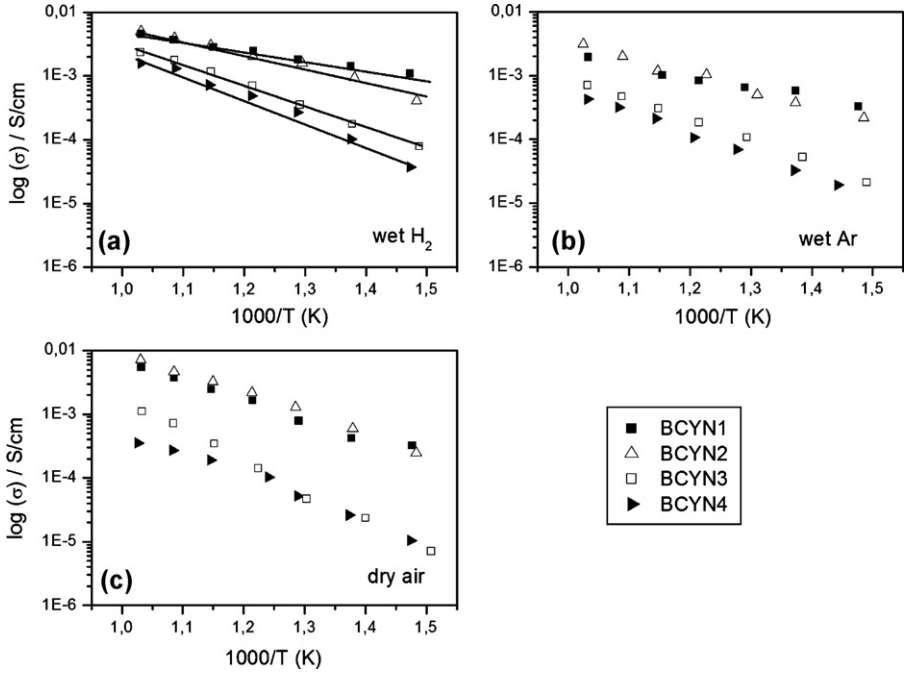

Fig. 7. Arrhenius plot of conductivity of $BaCe_{0.9-x}Nb_xY_{0.1}O_{3-x}$ ($x = 0.03$, 0.06, 0.09, and 0.12) in H_2 wet (a), argon dry (b) and air dry (c).

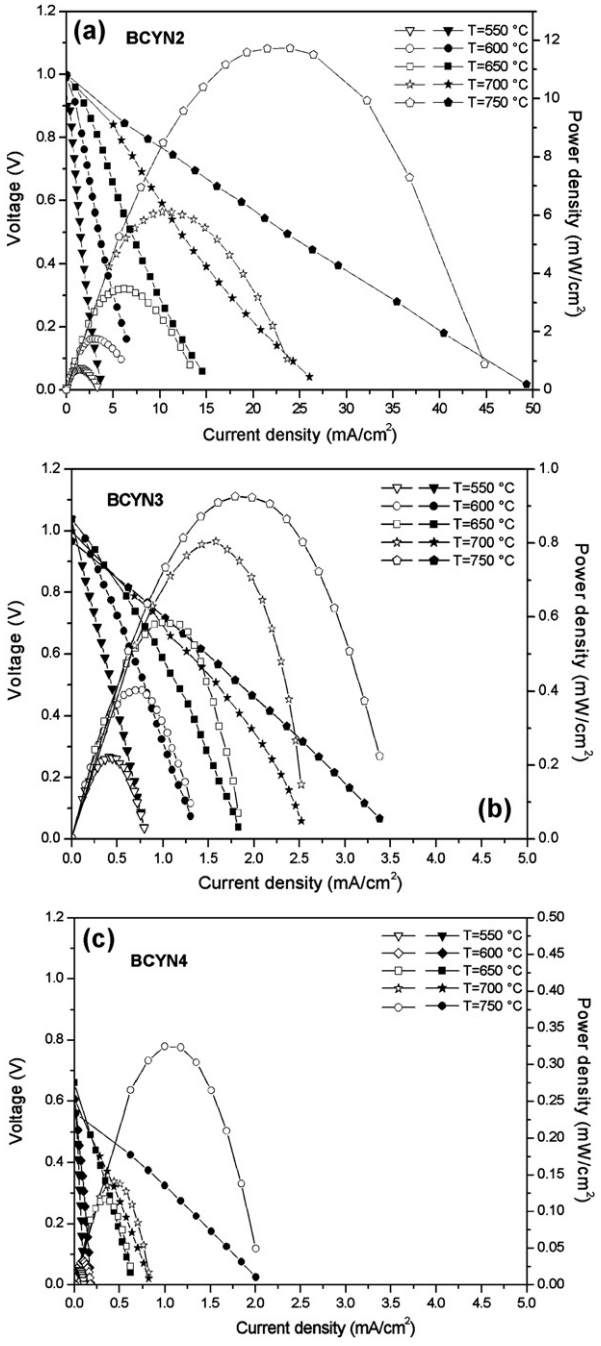

Fig. 8. *I–V* curves and power density output of Pt/$BaCe_{0.9-x}Nb_xY_{0.1}O_{3-x}$/Pt single cells measured at different temperatures in hydrogen–air fuel cell experiments: BCYN2 (a), BCYN3 (b), and BCYN4 (c).

Conductivity values were then calculated from the total resistance ($R_t = R_b + R_{gb}$) for all samples.

Fig. 7 shows Arrhenius plots in humidified H_2 (Fig. 7a), humidified Ar (Fig. 7b) and dry air (Fig. 7c). In all atmospheres, BCYN1 and BCYN2 have very close conductivity values, then a further increase of the Nb content (BCYN3 and BCYN4) significantly decreases conductivity. In all atmospheres, in fact, increasing the Nb-doping reflects into a decrease of oxygen vacancies.

The highest conductivity values were recorded in humidified H_2, a behavior typical of HTPCs. Activation energy values increased with increasing Nb content from 0.28 eV for BCYN1, to 0.46 eV for BCYN2, to 0.65 eV for BCYN3, eventually reaching a maximum value of 0.74 eV for BCYN4. The trend may be explained on the basis of the decreasing unit cell volume [27] in agreement with EXAFS and XRD analysis. The total conductivity decreased by increasing Nb content may also be related to the increase of the grain boundary contribution to resistance associated with the smaller grain size, as shown in the micrographs of Fig. 4.

At high temperatures (600–700 °C) in wet hydrogen, the Nb^{5+} concentration exerts a smaller influence on the overall conductivity than at lower temperatures (400–600 °C) in the whole series of samples. Differences in σ values become less significant most likely because of arising of n-type contribution as already reported in the literature [20].

The same effect is revealed in humidified Ar atmosphere (Fig. 7b) and may be ascribed as the reason of the higher slope observed for BCYN3 and BCYN4 with respect to BCYN1 and BCYN2, which also show an overall higher conductivity.

The conductivities of BCYN1 and BCYN2 in dry air at high temperatures (600–700 °C) are comparable to those measured in wet H_2 although conduction mechanism is certainly different and related to oxygen vacancies even though a p-type electronic contribution to conductivity cannot be excluded [28–32].

Fig. 8a–c shows the *I–V* and power density curves of Pt/$BaCe_{0.9-x}Nb_xY_{0.1}O_{3-x}$/Pt single cells for $x = 0.06$, 0.09 and 0.12 measured at different temperatures in hydrogen–air fuel cell experiments. The open-circuit voltage (OCV) in the BCNY2 based cell was about 1 V at all investigated temperatures suggesting that no gas leakages occurred through the electrolyte, in agreement with SEM analysis (Fig. 4). In the BCYN3 based cell the OCV was close to theoretical value in the temperature range between 550 and 650 °C, then at 700 and 750 °C the OCV decreased due to the arising electronic contribution. At variance with what observed for BCNY2 and BCNY3 equipped cells, the BCYN4 based cell showed a dramatic drop in OCV at all investigated temperatures. This feature can be justified by the presence of some gas leakages due to inferior sintering behavior also shown by the SEM image (Fig. 4).

The maximum power density was recorded at 750 °C for the BCYN2 based cell, reaching a value of about 12 mW cm^{-2}, i.e. the same order of magnitude measure for undoped BCY electrolytes [33,34]. At all temperatures the maximum power density decreased by increasing Nb content in the electrolyte. At 750 °C the maximum power density values were 11.7, 0.9, 0.3 mW cm^{-2} for BCY2, BCYN3, and BCYN4, respectively. The abrupt decrease in power density observed going from BCY2 to BCY3, reflects the observed drop in conductivity. The decrease of proton concentration due to the insertion of a 0.09 mol. amount of a pentavalent species in the BCY B site almost neutralizes the anion vacancy brought about by Y^{3+}, drastically reducing the electrochemical performance.

4. Conclusions

Crystalline and homogeneous powders of $BaCe_{0.9-x}Nb_xY_{0.1}O_{3-x}$ ($x = 0.03$, 0.06, 0.09 and 0.12) were prepared by citrate–nitrate autocombustion process. X-ray absorption and XRD demonstrated that the B site of BCY electrolyte was co-doped with Nb^{5+} producing a structural contraction around niobium and local disorder increasing with Nb concentration. Co-doping was effective in improving the chemical stability of the perovskite structure against carbonation. As a result of the increased basic character of the doped oxides, the sample with the highest Nb content, BCYN4, showed the highest stability in pure CO_2.

Conductivity measurements were carried out in different atmospheres: BCYN1 and BCYN2 showed the highest conductivity values and lowest activation energy in all atmospheres in agreement with the decreased unit cell volume and superior sintering behavior. Best fuel cell performance were obtained with $BaCe_{0.84}Nb_{0.06}Y_{0.1}$, which resulted to be the best electrolyte among those examined in terms

of chemical stability and balanced ratio of oxygen vacancies and proton concentration.

Acknowledgments

This work has been supported by the Ministry of University and Research (MiUR) of Italy (PRIN 2008 Project "PC-SOFCs, Protonic Conductors Solid Oxide Fuel Cells based on nanostructured proton conductors: from materials synthesis to prototype fabrication").

The authors thank Ms Cadia D' Ottavi for her valuable technical assistance.

References

[1] K. Katahira, Y. Kohchi, T. Shimura, H. Iwahara, Solid State Ionics 138 (2000) 91–98.
[2] K.D. Kreuer, St. Adams, W. Munch, A. Fuchs, U. Klock, J. Maier, Solid State Ionics 145 (2001) 295–306.
[3] N. Taniguchi, K. Hatoh, J. Niikura, T. Gamo, Solid State Ionics 53–56 (1992) 998–1003.
[4] G. Ma, T. Shimura, H. Iwahara, Solid State Ionics 110 (1998) 103–110.
[5] D. Shima, S.M. Haile, Solid State Ionics 97 (1997) 443–455.
[6] N. Zakowsky, S. Williamson, J.T.S. Irvine, Solid State Ionics 176 (2005) 3019–3026.
[7] S.V. Bhide, A.V. Virkar, J. Electrochem. Soc. 146 (1999) 2038–2044.
[8] L. Bi, Z. Tao, C. Liu, W. Sun, H. Wang, W. Liu, J. Membr. Sci. 336 (2009) 1–6.
[9] K. Xie, R. Yan, X. Xu, X. Liu, G. Meng, J. Power Sources 187 (2009) 403–406.
[10] K. Xie, R. Yan, X. Chen, S. Wang, Y. Jiang, X. Liu, G. Meng, J. Alloys Compd. 473 (2009) 323–329.
[11] P. Pasierb, M. Wierzbicka, S. Komornicki, M. Rekas, J. Power Sources 194 (2009) 31–37.
[12] H. Matsumoto, Y. Kawasaki, N. Ito, M. Enoki, T. Ishihara, Electrochem. Solid State Lett. 10 (2007) B77–B80.
[13] E. Fabbri, A. D'Epifanio, E. Di Bartolomeo, S. Licoccia, E. Traversa, Solid State Ionics 179 (2008) 558–564.
[14] S.S. Bhella, T. Fürstenhaupt, R. Paul, V. Thangadurai, Inorg. Chem. (2011) 6493–6499.
[15] K.H. Ryu, S.M. Haile, Solid State Ionics 125 (1999) 355–367.
[16] A.K. Azad, J.T.S. Irvine, Solid State Ionics 178 (2007) 635–640.
[17] C. Zuo, S. Zha, M. Liu, M. Hatano, M. Uchiyama, Adv. Mater. 18 (2006) 3318–3320.
[18] S. Ricote, N. Bonanos, G. Caboche, Solid State Ionics 180 (2009) 990–997.
[19] E. Fabbri, D. Pergolesi, A. D'Epifanio, E. Di Bartolomeo, G. Balestrino, S. Licoccia, E. Traversa, Energy Environ. Sci. 1 (2008) 355–359.
[20] K.D. Kreuer, Annu. Rev. Mater. Res. 33 (2003) 333–359.
[21] M. Zunic, L. Chevallier, F. Deganello, A. D'Epifanio, S. Licoccia, E. Di Bartolomeo, E. Traversa, J. Power Sources 190 (2009) 417–422.
[22] A.L. Ankudinov, B. Ravel, J.J. Rehr, S.D. Conradson, Phys. Rev. B 58 (1998) 7565–7576.
[23] K.D. Klementev, J. Phys. D: Appl. Phys. 34 (2001) 209–214.
[24] F. Giannici, A. Longo, A. Balerna, K.D. Kreuer, A. Martorana, Chem. Mater. 21 (2009) 2641–2649.
[25] F. Giannici, A. Longo, A. Balerna, A. Martorana, Chem. Mater. 21 (2009) 597–603.
[26] F. Giannici, A. Longo, A. Balerna, K.-D. Kreuer, A. Martorana, Chem. Mater. 19 (2007) 5714–5720.
[27] A.R. Pottera, R.T. Baker, Solid State Ionics 177 (2006) 1917–1924.
[28] H. Uchida, N. Maeda, H. Iwahara, Solid State Ionics 11 (1983) 117–124.
[29] N. Bonanos, B. Ellis, K.S. Knight, M.N. Mahmood, Solid State Ionics 35 (1989) 179–188.
[30] N. Fukatsu, N. Kurita, T. Yajima, K. Koide, T. Ohashi, J. Alloys Compd. 231 (1995) 706–712.
[31] T. He, K.D. Kreuer, Yu.M. Baikov, J. Maier, Solid State Ionics 95 (1997) 301–308.
[32] A. Mitsui, M. Miyayama, H. Yanagida, Solid State Ionics 22 (1987) 213–217.
[33] P.A. Stuart, T. Unno, J.A. Kilner, S.J. Skinner, Solid State Ionics 179 (2008) 1120–1124.
[34] W. Suksamai, I.S. Metcalfe, Solid State Ionics 178 (2007) 7–10.